AIAA 80-0805R

Effect of Aeroelastic Considerations on Seasat-A Payload Shroud Design

J. Peter Reding* and Lars E. Ericsson†
Lockheed Missiles & Space Co., Inc., Sunnyvale, Calif.

The Seasat-A is an experimental satellite that was launched into orbit by an Atlas/Agena booster. The original Seasat-A launch configuration featured a hammerhead payload shroud that endangered the vehicle's structural integrity. A quasisteady analysis of the aeroelastic stability of the booster revealed two potentially dangerous unsteady flow phenomena that could cause aeroelastic instability. In order to eliminate all possibility of aeroelastic instability, the payload shroud was redesigned. The hammerhead was eliminated and a biconic nose was used to eliminate the shoulder separation. The redesigned payload shroud had the added bonus of increasing booster performance through reduced drag. The Seasat-A with the redesigned payload shroud flew successfully with no indication of aeroelastic instability.

Nomenclature

a = freestream sonic speed
B = $(\rho U^2 S)/2\bar{m}$
c = reference length, Atlas diameter
D = shroud diameter
D_s, D_a = damping parameters, Eq. (1)
d = Agena diameter
f = frequency, Hz
K = equivalent aerodynamic spring, Eq. (1)
L = Agena length
L_1 = axial location of 1st node relative to hammerhead shoulder (Fig. 2)
M = Mach number U/a
m = pitching moment; coefficient, $C_m = (m/qSc)$
$\bar{m}$ = generalized mass
N = normal force; coefficient, $C_N = N/qS$
p = local pressure; coefficient, $C_p = (p - p_\infty)/q$
p_∞ = freestream static pressure
q = dynamic pressure; $q = (\rho U^2)/2$
$q(t)$ = normalized coordinate
S = reference area, $S = (\pi c^2)/4$
t = time
U = freestream velocity
$\bar{U}$ = flow convection speed
x = axial coordinate
z = normal coordinate
α = angle of attack
$\bar{\alpha}$ = generalized angle of attack
β = parameter defined by Eq. (9)
Δ = increment
θ = inertial attitude
ϕ = normalized modal deflection
ϕ' = normalized modal slope
ψ = phase angle; $\psi = \omega t$
$\omega, \bar{\omega}$ = circular frequency; $\omega = 2\pi f, \bar{\omega} = \omega c/U$
ξ = normalized axial coordinate, $\xi = x/c$
ζ = normalized normal coordinate, $\zeta = z/c$
$\bar{\zeta}$ = equivalent viscous damping of the structure, $(2\bar{\zeta} = g)$

Subscripts

a = attached flow
D = condition of critical flow
N = nose-cylinder juncture
s = separated flow
T = tail or booster base
o = trim condition
1, 2, etc. = numbering subscript

Presented as Paper 80-0805 at the AIAA/ASME/ASCE/AHS 21st Structures, Structural Dynamics & Materials Conference, Seattle, Wash., May 12-14, 1980; submitted July 9, 1980; revision received Dec. 12,1980.

*Staff Engineer. Associate Fellow AIAA.
†Senior Consulting Engineer. Associate Fellow AIAA.

Introduction

THE Seasat-A is an experimental satellite designed to explore the feasibility of using a network of multiple satellites to monitor the world's oceans on a near-real-time basis. The satellite was lofted into orbit atop an Atlas/Agena booster. The original 84-in. diameter Seasat-A payload shroud, designed for minimum weight, just covered the payload and was faired to the smaller-diameter Agena upper stage with a conic frustum (Fig. 1). The Agena in turn was faired to the larger-diameter Atlas first stage via another conic frustum. The resulting hammerhead boost configuration violated two of the three design criteria for hammerheads specified some years ago by NASA[1] to avoid the aeroelastic stability problems experienced by early hammerhead configurations. This, of course, caused concern for the structural integrity of Seasat. Therefore, the aeroelastic stability of the booster was analyzed in order to determine how serious the aeroelastic stability problems were and how to cope with them.

The aeroelastic problems caused by hammerheads involve separated flow.[2] Quasisteady techniques have been used successfully in the past to treat the aeroelastic problems caused by flow separation.[2-13] Quasisteady techniques that account for the flowfield time lag in separated flow have been used to determine the effects of flow separation on the aeroelastic stability of the Apollo-Saturn I boosters.[3,4] The technique did so well in predicting the aeroelastic characteristics of a fully elastic wind-tunnel model of the Apollo-Saturn I[5,6] that it was the only means used to assess the aeroelastic stability of all other Apollo-Saturn boosters.[7-9] Since then, the quasisteady technique has been used to analyze the aeroelastic stability of a number of vehicles dominated by flow separation.[10-13] The present paper reviews the application of this technique to the Seasat-A booster and how it led to the shroud redesign that eliminated the aeroelastic problems of the original configuration.

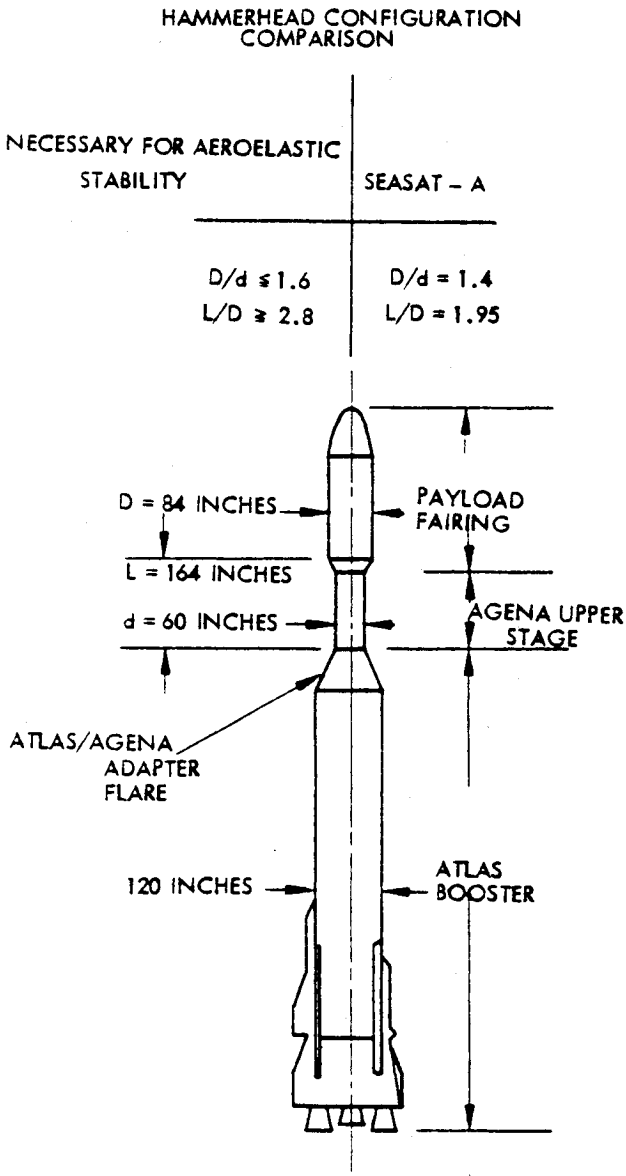

Fig. 1 Seasat-A configuration.

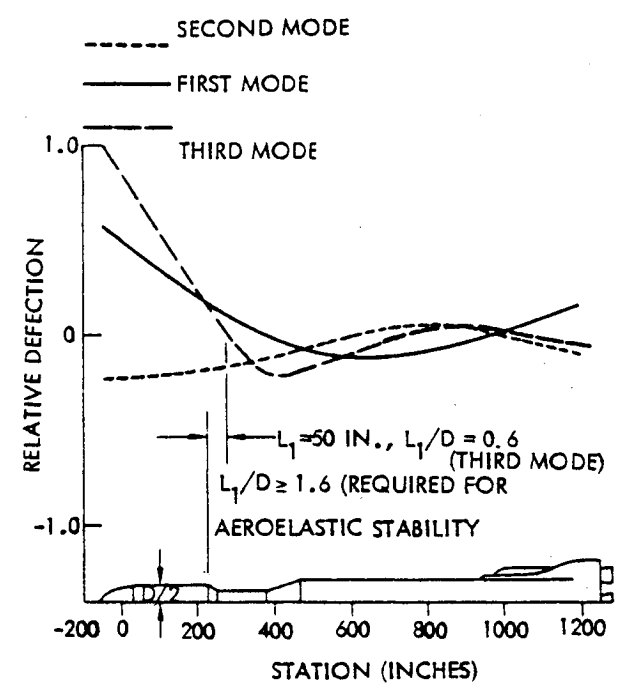

Fig. 2 Seasat-A mode shapes.

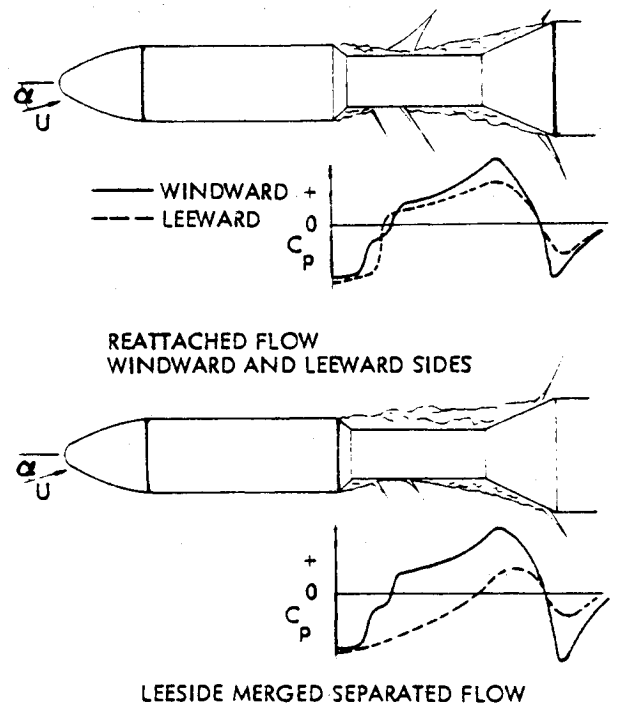

Fig. 3 Comparison of separated flow types.

Shroud Aerodynamics

The original Seasat-A launch configuration violated two criteria for the design of hammerhead configurations specified by NASA to avoid aeroelastic instability.[1] The $L/D=1.95$ gap between the base of the hammerhead shroud and the following Atlas/Agena interstage flare (Fig. 1) should have been at least 2.8 payload-shroud diameters long ($L/D=2.8$) to meet the criterion. Furthermore, the third free-free bending mode violated the criterion for the location of the forward node relative to the hammerhead. The design criterion specifies that the node should be at least 1.6 shroud diameters aft of the hammerhead base ($L_1/D=1.6$). For the original Seasat-A, the first node of the third mode was only 0.6 shroud diameters aft of the hammerhead ($L_1/D=0.6$ in Fig. 2), thus, the hammerhead appeared to be a prime candidate as a source of aeroelastic instability.

The flow phenomenon that endangered the aeroelastic stability of the hammerhead configuration was the sudden merging of the hammerhead wake with the flare-induced separation forward of the Atlas/Agena interstage frustum. Consider the vehicle flying at a low supersonic Mach number, at an angle of attack where the hammerhead wake on the leeward side just reattaches on the following cylinder and then immediately reseparates because of the adverse pressure gradient caused by the flare (Fig. 3a). Any increase in the angle of attack will cause the boundary layer to thicken on the leeside due to forebody crossflow effects. The leeside separation point of the flare-induced separation will move forward in response to the boundary layer thickening[14] and will merge with the hammerhead wake as illustrated in Fig. 3b. The pressures on the leeside in the region of merged separation will be considerably less than for the reattached-reseparated flow that occurs on the windward side (Fig. 3). The result will be a sudden discontinuous normal load on the cylinder and flare aft of the hammerhead.

Dynamically, the discontinuous aerodynamic load will lag the vehicle motion because of the finite-flow convection speed in the hammerhead boundary layer and wake. That is, crossflow effects will thicken the leeside boundary layer on the payload shroud. The boundary-layer thickening will progress downstream at the boundary-layer convection speed. Thus, the merged-flow separation load will lag the vehicle attitude by the time increment $\Delta t=(x_N-x_S)/\bar{U}$ where (x_N-x_S) is the distance between the lumped crossflow influence

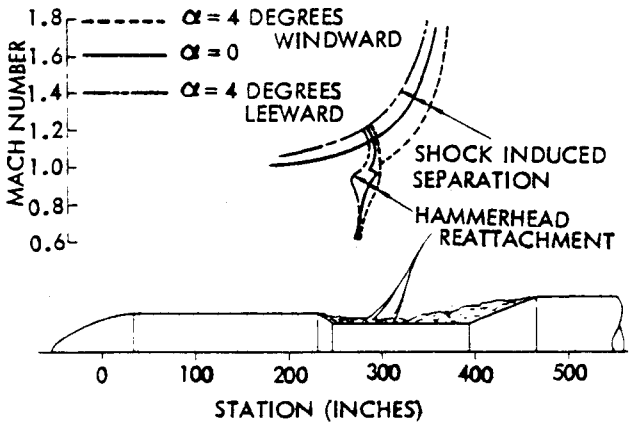

Fig. 4 Merging of hammerhead and shock-induced flow separations.

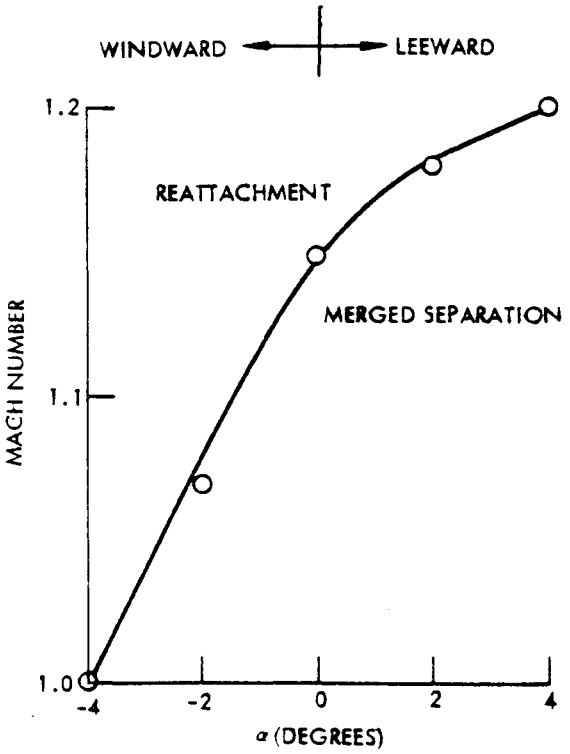

Fig. 5 Merged separation boundary.

point (x_N) and the location of the separated-flow load element (x_S), and $\bar{U} = 0.8U$ is the boundary-layer convection speed.[15]

By now it has been well established that a flowfield time lag causes a statically stabilizing aerodynamic load to be dynamically destabilizing and vice versa.[2-13] Thus, for the critical third mode, the portion of the sudden merged-separation load aft of the forward node will be undamping (compare Figs. 2 and 3).

Unfortunately, no wind-tunnel data were obtained on the original Seasat-A configuration. Thus, a precise definition of the merged separation and the magnitude of the loads involved was not possible. The flight conditions for merged separation were estimated from wind-tunnel results for similar configurations. The location of the hammerhead wake reattachment was taken from Ref. 16 and adjusted for hammerhead diameter ratio (D/d in Fig. 1). The extent of the flare-induced separation was taken from Ref. 17 for a 23-deg flare.‡ The intersection of these boundaries (Fig. 4) defines the conditions for merged flow. These critical flight conditions are shown in Fig. 5. When the vehicle is flying near the

‡The Atlas/Agena interstage frustum is a 25-deg flare.

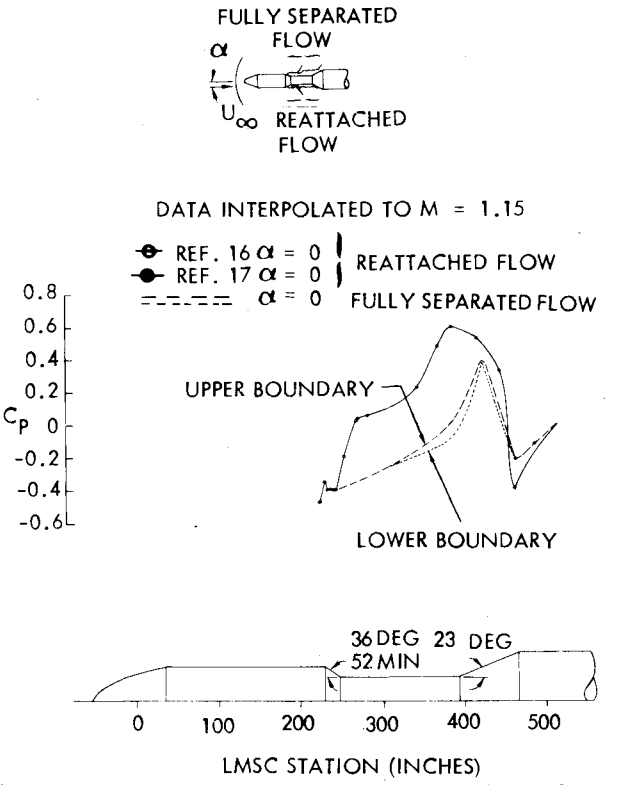

Fig. 6 Hammerhead pressure due to sudden windward reattachment.

critical condition, small changes in the angle of attack, such as those caused by elastic oscillations of a free-free bending mode, will cause merged separation to occur in an on-off fashion. Figure 5 shows that for $M = 1.15$ and $\alpha = 0$ merged separation occurs on the leeward side and reattachment occurs on the windward side. For $M > 1.15$, reattachment occurs on both windward and leeward sides at $\alpha = 0$ and persists until α is increased to its critical (positive) value (where merged separation will occur on the leeside). Conversely, for $M < 1.15$, merged separation occurs on both windward and leeward sides at $\alpha = 0$ and persists until α is decreased to its critical (negative) value (where reattachment suddenly occurs on the windward side).

The merged-separation boundary in Fig. 5 only approximates the actual flight boundary. This is primarily because the boundaries were taken from wind-tunnel data where the flare-induced separation was not preceded by a reattaching hammerhead wake. The low-energy portion of the hammerhead boundary layer will be trapped in the wake recirculation region; thus, the boundary layer approaching the shock-induced separation forward of the interstage flare will be relatively stronger for the hammerhead configuration. This causes the shock-induced separation to occur closer to the flare, which will effectively move the merged-separation boundary in Fig. 5 to the right. This however, does not significantly change the likelihood of encountering merged separation because vehicle angles of attack up to 4 deg can occur throughout the low-supersonic Mach range.

The loads caused by the sudden merged separation were also estimated from wind-tunnel data available in the literature. The windward-side pressure distribution for reattached flow (Fig. 6) was obtained from interpolation of the data of Refs. 16 and 17. The leeside pressures were estimated by recognizing the similarity between the sudden merged separation on the Seasat-A to the shoulder reseparation on the Apollo-Saturn I, as well as to the sudden jump from shock-induced separation to nose-induced separation on cylinder-flare bodies.[18,19] These data determined the leeside flare pressures (within the bounds shown in Fig. 6) which were faired into the hammerhead-wake pressure level. It is interesting to note that the hammerhead wake

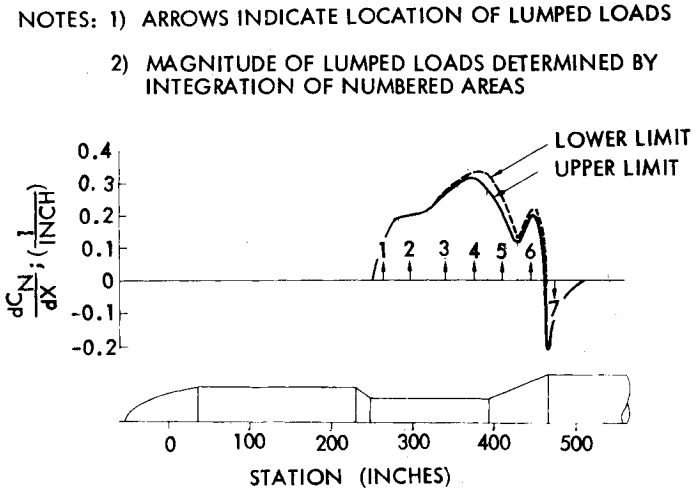

Fig. 7 Distribution of discontinuous normal force due to sudden windward reattachment.

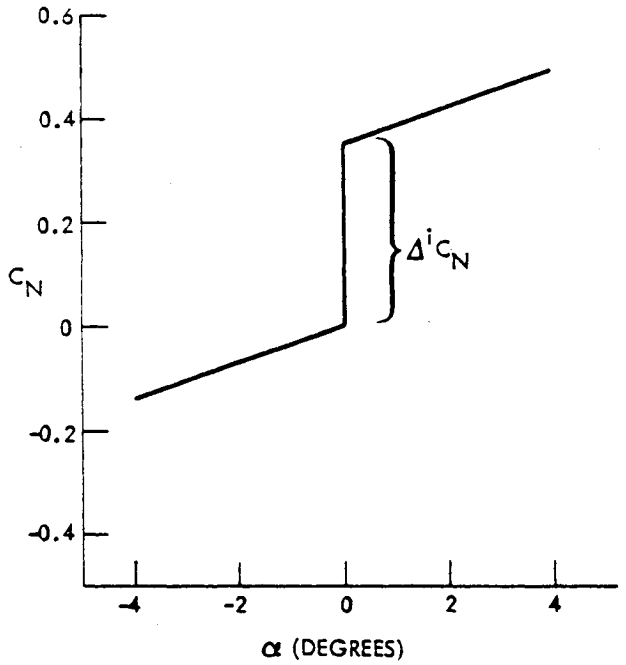

Fig. 8 Estimated normal force, $M = 1.15$.

pressure coefficient ($Cp = -0.4$) seems to be the minimum achievable transonic separated-flow pressure coefficient for a variety of bodies of revolution; including hammerhead wakes,[16,20] nose-induced separation,[16,18,19] and shoulder separation.[18] The negative load aft of the Atlas/Agena interstage flare is of the same magnitude as has been observed aft of flares preceded by similar sized runs of flow separation.[18,19]

The resulting windward- and leeward-side pressure distributions in Fig. 6 were integrated, assuming a cosine circumferential pressure distribution, to give the normal-force distribution shown in Fig. 7. This distribution was approximated by seven lumped-load vectors (Fig. 7) for the quasisteady aeroelastic stability analysis, as will be discussed in detail in the following section. Superimposing the integrated, merged-separation jump load on the continuous attached-flow normal force characteristics for Seasat-A gives the normal-force characteristics shown in Fig. 8. For $M = 1.15$ the discontinuous normal-force jump due to the merged leeside separation is significant. It is roughly equivalent to the normal force generated over the rest of the body by an 8-deg angle-of-attack change. This is in basic agreement with the discontinuous load changes observed on cylinder flare bodies dominated by separated flow.[18]

The sudden flow separation that occurs aft of slender noses[21,22] at high transonic speeds also posed a potential threat to the Seasat-A aeroelastic stability. In this case, the terminal normal shock that occurs aft at the nose-shoulder over-expansion jumps to the shoulder at some critical α. This causes a discontinuous negative shoulder load that is statically stabilizing and undamping for the lowest three Seasat-A bending modes, just as it was aerodynamically undamping for the Saturn I with a Jupiter nose fairing.[23] Fortunately, the Seasat-A only realized this sudden separation for 0.26 seconds on the worst case. This allows only 1.64 cycles of oscillation for the high-frequency third mode, hardly enough time to achieve the limit cycle amplitude. Thus, sudden shoulder separation was judged not to pose a viable threat to the Seasat-A aeroelastic stability.

Aeroelastic Analysis

The equation of motion of the elastic vehicle describing single degree-of-freedom bending oscillations can be written[3,4]

$$\bar{m}\left[\ddot{q}(t) + 2\omega\left(\bar{\xi} - \frac{B}{2\omega U}(D_s + D_a)\right)\dot{q}(t) + \omega^2\left(1 - \frac{B}{\omega^2}(K_s + K_a)\right)q(t)\right] = P(t) \tag{1}$$

where $P(t)$ is the buffeting force input.

One requirement for stability is that the coefficient of $\dot{q}(t)$ cannot be negative; i.e.,

$$\bar{\xi} - \frac{B}{2\omega U}(D_s + D_a) \geq 0 \tag{2}$$

where D_s and D_a are the aerodynamic damping derivatives due to separated and attached flow, respectively (a negative coefficient is damping). $\bar{\xi}$ is the structural damping as a fraction of critical damping, and $B/2\omega U = \rho US/4\omega\bar{m}$ puts the aerodynamic damping into the same form as the structural damping. For a discontinuous aerodynamic load the damping is obtained by integrating over one cycle.[8,11,12,23]

$$D_s = \frac{\phi(\xi_s)c}{\pi\Delta q\tilde{\omega}} \int_{\beta}^{2\pi+\beta} C_N(\psi)\cos\psi \, d\psi \tag{3}$$

For the typical discontinuous lumped-load vector caused by merged separation (Fig. 9), the generalized angle of attack is the following:

$$\tilde{\alpha} = \alpha_o + \theta - \dot{z}/U \tag{4}$$

The sudden merged separation is the result of the crossflow at the lumped-crossflow influence point (the nose-cylinder shoulder) $x_N = \xi c$ (in Fig. 9).

$$\tilde{\alpha} = \alpha_o + \theta_N(t - \Delta t) - \dot{z}_N(t - \Delta t)/U \tag{5}$$

With the elastic body coordinate system (Fig. 9)

$$\theta_N(t - \Delta t) = \phi'(\xi_N)q(t - \Delta t)$$

$$\dot{z}_N(t - \Delta t) = \phi(\xi_N)\dot{q}(t - \Delta t) \tag{6}$$

where $q = \Delta q \sin\omega t$ and $\Delta t = c(\xi_S - \xi_N)/\bar{U}$ is the time lag. $\bar{U} = 0.8\bar{U}$ is the convective speed within a turbulent boundary

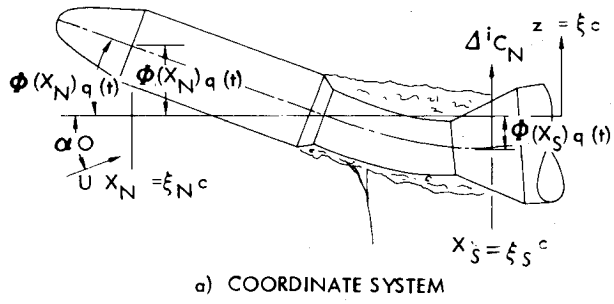

a) COORDINATE SYSTEM

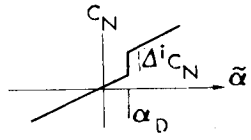

b) INDUCED LOAD

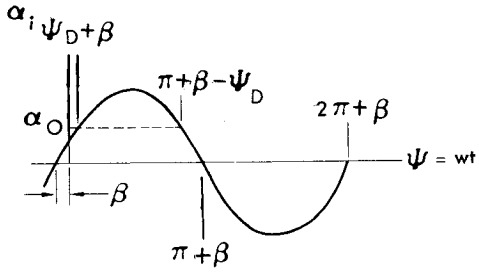

c) INSTANTANEOUS ANGLE-OF-ATTACK

Fig. 9 Definition of terms.

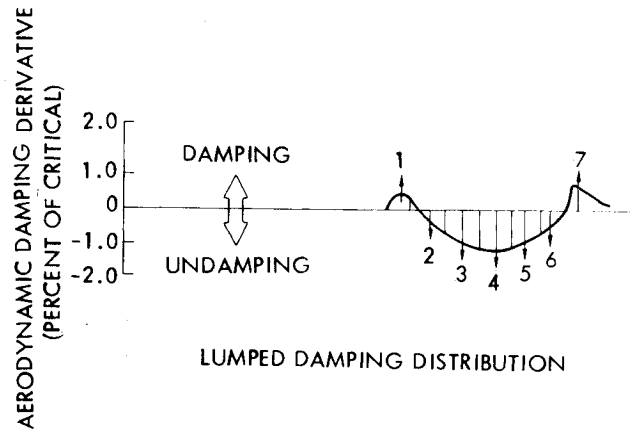

LUMPED DAMPING DISTRIBUTION

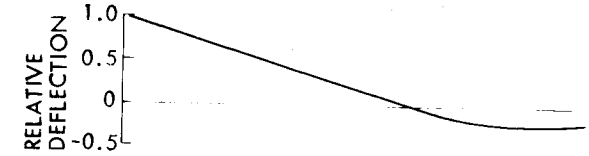

FORWARD PORTION OF THIRD MODE

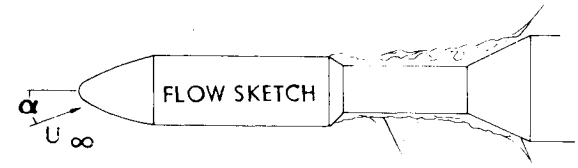

Fig. 10 Aerodynamic damping distribution in merged flow region: $\Delta q = 0.1$ ft, $M = 1.15$, $\alpha = 0$.

layer[15] therefore,

$$\tilde{\alpha} = \alpha_o + \phi'(\xi_N)\Delta q[\sin\omega t\cos\omega\Delta t - \cos\omega t\sin\omega\Delta t]$$

$$-[\phi(\xi_N)/U]\Delta q\omega[\cos\omega t\cos\omega\Delta t + \sin\omega t\sin\omega\Delta t] \quad (7)$$

or

$$\tilde{\alpha} = \alpha_o + \sec\beta[\phi'(\xi_N)\cos\omega\Delta t$$

$$-\phi(\xi_N)(\omega/U)\sin\omega\Delta t]\Delta q\sin(\psi-\beta) \quad (8)$$

where $\psi = \omega t$ and

$$\beta = \tan^{-1}\left\{\frac{\phi'(\xi_N)\sin\omega\Delta t + \phi(\xi_N)(\omega/U)\cos\omega\Delta t}{\phi'(\xi_N)\cos\omega\Delta t - \phi(\xi_N)(\omega/U)\sin\omega\Delta t}\right\} \quad (9)$$

Thus, for the discontinuity that occurs at $\tilde{\alpha} = \alpha_D$

$$\psi_D - \beta = \sin^{-1}\left\{\frac{(\alpha_D - \alpha_o)\cos\beta}{\Delta q\phi'(\xi_N)\cos\omega\Delta t - \phi(\xi_N)(\omega/U)\sin\omega\Delta t}\right\} \quad (10)$$

The dominating separation-induced effect is the discontinuous load change due to the sudden merged separation (Fig. 3). Applying Eq. (3) gives

$$D_s = \frac{2\phi(\xi_s)c}{\pi\Delta q\tilde{\omega}}\int_{\psi_D}^{\pi+2\beta-\psi_D}\Delta C_N\frac{\tilde{\alpha}}{|\tilde{\alpha}|}\cos\psi d\psi \quad (11)$$

Integrating gives

$$D_s = -[2\phi(\xi_s)c/\pi\Delta q\tilde{\omega}]\Delta C_N\sin\beta\cos(\psi_D - \beta) \quad (12)$$

The attached-flow damping derivative is from first-order theory.[24]

$$D_a = -C_{N\alpha}[\phi(\xi_T)]^2 \quad (13)$$

$C_{N\alpha}$ is the attached-flow, normal-force derivative of the boost configuration, and $\phi(\xi_T)$ is the modal deflection at the booster base.

The contribution of the merged separation to the modal damping derivative is found from the integration of Eq. (12) using the lumped-load approximation to the merged-separation-induced load distribution (Fig. 7). The aerodynamic damping in percent of critical is found from Eq. (3) by combining attached- and separated-flow aerodynamic damping derivatives.

One can see that for the third mode, where $\phi(\xi_s) < 0$ for the bulk of the merged-load distribution (compare Figs. 2 and 7), aerodynamic undamping will result if $|D_s| > |D_a|$. Actually $D_s \to \infty$ for infinitesimal amplitude modal oscillations ($\Delta q = 0$) at $\alpha_o = \alpha_D$. When the oscillation amplitude becomes finite, D_s also becomes finite until $D_s \to 0$ for large Δq and the aerodynamic damping approaches the attached-flow value D_a.

Figure 10 shows the aerodynamic damping distribution over the portion of the vehicle that is influenced by the merged separation for the third bending mode with $\Delta q = 0.1$ ft. Comparison with Fig. 7 shows the effect of the local modal deflection on the damping contribution from the separated flow. Note that positive loads aft of the first node [where $\phi(\xi_S) < 0$], which act to return the mode to the null position (are statically stabilizing), contribute undamping dynamically; thus illustrating the basic opposition between static and dynamic stability for separation-induced loads.

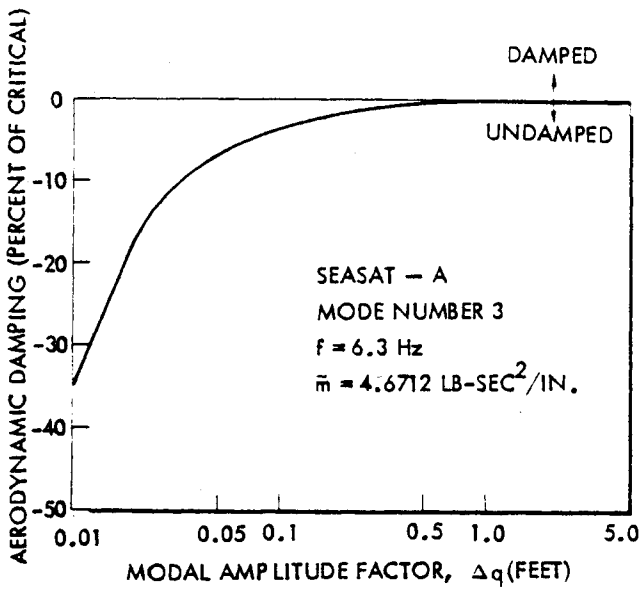

Fig. 11 Effect of modal amplitude on aerodynamic damping.

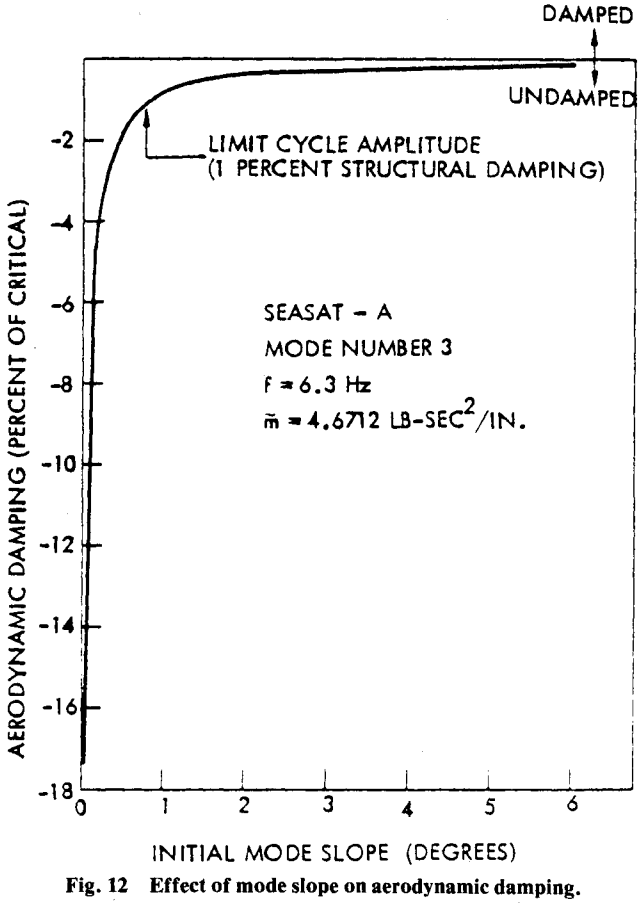

Fig. 12 Effect of mode slope on aerodynamic damping.

Discussion of Results

The estimated value for the structural damping at the critical third mode of the Seasat-A was 1% of critical. Therefore the practical limit cycle is determined by

$$\zeta = 0.01 = -(\rho US/4\omega\bar{m})(D_a + D_s) \qquad (14)$$

This gives a limit-cycle oscillation amplitude factor of $\Delta q_{\text{limit}} = 0.35$ ft for the third mode of the Seasat-A configuration at $\alpha = 0$ and $M = 1.15$ (Fig. 11). This is representative of the limit-cycle amplitudes that will occur throughout the merged-flow region. In order to define the impact of the limit cycle, one would need to dimensionalize the mode shape by the multiplication of $\phi(\xi)$ by Δq_{limit} and then proceed with a stress analysis to determine if structural failure will occur. However, one can make some judgment of the seriousness of the limit cycle from experience with similar vehicles. For example, a 0.25-deg mode slope at the nose of the third mode of the Saturn 203 vehicle was enough to endanger its structural integrity.[8] Using the estimated structural damping of 1% of critical gives a 0.8 deg mode slope at the nose of the Seasat-A for the critical third mode (Fig. 12). Because it is doubtful that the equivalent viscous structural damping can be estimated better than within ±50%, limit-cycle oscillations giving nose slopes between 0.5 and 1.5 deg are possible. Based on the Saturn experience, this is dangerously large.

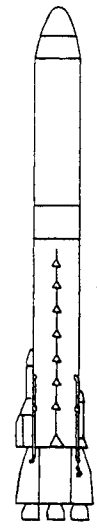

Fig. 13 Final Seasat-A configuration.

Of course, one must consider the probability of maintaining the critical flight conditions long enough to achieve the limit-cycle amplitude. The $-4 \le \alpha \le 4$ deg range of the merged-separation boundary is within the maximum angle-of-attack expected for Seasat-A.[25] The maintaining of the critical α-M history of Fig. 5 long enough to achieve limit-cycle oscillations undoubtedly has some finite probability. The judgment was made that one could not accept a design that had any chance of experiencing aeroelastic instability. The payload shroud had to be redesigned.

Two alternative shroud modifications were suggested: 1) lengthening the 60-in. diameter Agena section (Fig. 1) to achieve an $L/D \ge 2.8$ and a $L_1/D = 1.6$ to meet the NASA design criteria; 2) elimination of the hammerhead altogether.

The former increased the bending loads at the Atlas/Agena interstage to unacceptable levels. Therefore, it was decided to eliminate the hammerhead by enclosing both the payload and the Agena upper stage in a fairing that had a diameter equal to the booster diameter (Fig. 13). In addition, the redesigned shroud featured a biconic nose that has been shown to eliminate the sudden shoulder separation.[8,23] Thus, the new shroud eliminated all separation-induced unsteady-flow phenomena that could affect the aeroelastic stability. The new shroud had the added advantage of reducing the drag by eliminating the base drag on the hammerhead and the pressure drag on the Atlas/Agena interstage frustum. These drag reductions more than offset the additional pressure drag on the larger diameter nose and the added skin friction drag of the larger cylinder.

The redesigned payload shroud flew successfully boosting the satellite into orbit on June 26, 1978.

Concluding Remarks

An analysis of the Seasat-A aeroelastic stability has reaffirmed that hammerhead payloads must be carefully designed in order to avoid aeroelastic instability. One should

either follow the NASA design criteria or conduct a careful, detailed analysis to ensure aeroelastic stability. Furthermore, the drag reduction achieved with the redesigned shroud indicates that one should carefully consider the trade-off between drag and weight penalties before selecting a hammerhead payload.

Perhaps the most important lesson to be learned from the Seasat-A is the advisability of examining booster aeroelastic stability early in the design. This is particularly true where flow separation dominates the booster aerodynamics. Early analysis means early identification of aeroelastic problems and avoids the necessity of redesign late in the program when it is the most costly.

Acknowledgment

This work was accomplished as part of the Seasat-A development and integration effort under Contract NAS 3-20638D.

References

[1] "NASA Space Vehicle Design Criteria, Volume II: Structures, Part B: Loads and Structural Dynamics, Chapter 3: Launch and Exit, Section I: Buffeting," NASA SP-8001, May 1964.

[2] Woods, P. and Ericsson, L. E., "Aeroelastic Considerations in a Slender, Blunt-Nose, Multistage Rocket," *Aerospace Engineering,* May 1962, pp. 42-51.

[3] Ericsson, L. E. and Reding, J. P., "Report on Saturn I-Apollo Unsteady Aerodynamics," Lockheed Missiles & Space Co., Inc. Report, LMSC-A650215, Feb. 1964.

[4] Ericsson, L. E. and Reding, J. P., "Analysis of Flow Separation Effects on the Dynamics of a Large Space Booster," *Journal of Spacecraft and Rockets,* Vol. 2, July-Aug. 1965, pp. 481-490.

[5] Hanson, P. W. and Doggett, R. V. Jr., "Aerodynamic Damping and Buffet Response of an Aeroelastic Model of the Saturn I, Block II Launch Vehicle," NASA TM D2713, March 1965.

[6] Rainey, A. G., "Progress in the Launch Vehicle Buffeting Problem," *Journal of Spacecraft and Rockets,* Vol. 2, May-June 1965, pp. 289-299.

[7] Ericsson, L. E. and Reding, J.P., "Dynamics of Separated Flow over Blunt Bodies," Technical Summary Report, LMSC 2-80-65-1, Dec. 1965.

[8] Ericsson, L. E., French, N. J., and Guenther, R. A., "The Aeroelastic Characteristics of the Saturn IB Launch Vehicle with Biconic Payload Shroud," LMSC M-37-65-1, June 1967.

[9] Ericsson, L. E. and Reding, J. P., " Technical Summary Report, Aeroelastic Characteristics of Saturn IB and Saturn V Launch Vehicles," LMSC M-37-67-5, Dec. 1967.

[10] Ericsson, L. E. and Reding, J. P., "Unsteady Airfoil Stall and Stall Flutter," NASA CR-111906 also LMSC A-6J-71-1, June 1971.

[11] Reding J. P. and Ericsson, L. E., "Aeroelastic Stability of the 747/Orbiter," *Journal of Spacecraft and Rockets,* Vol. 14, Oct. 1977, pp. 988-993.

[12] Reding, J. P. and Ericsson, L. E., "Effects of Flow Separation on Shuttle Longitudinal Dynamics and Aeroelastic Stability," *Journal of Spacecraft and Rockets,* Vol. 14, Dec. 1977, pp. 711-718.

[13] Reding, J. P., Guenther, R. A., and Richter, B. J., "Unsteady Considerations in the Design at a Drag-Reduction Spike," *Journal of Spacecraft and Rockets,* Vol. 14, Jan. 1977, pp. 54-60.

[14] Guenther, R. A., "Flow Separation Studies," LMSC L-87-66-1, Dec. 1966.

[15] Kistler, A. L. and Chen, W. S., "The Fluctuating Pressure Field in a Supersonic Turbulent Boundary Layer," Jet Propulsion Laboratory TR 32-277, Aug. 1962.

[16] Coe, C. F., "The Effects of Some Variations in Launch-Vehicle Nose Shape on Steady and Fluctuating Pressures at Transonic Speeds," NASA TM X-646, March 1962.

[17] Graham, F. J. and Butler, C. B., "Static Pressure Distribution on a 0.07-Scale Aerodynamic Model of the Atlas-Able IV at Free-Stream Mach Numbers from 0.50 to 1.6," Arnold Engineering Development Center, AEDC-TN-60-128, July 1960.

[18] Ericsson, L. E., "Separated Flow Effects on the Static and Dynamic Stability of Blunt Nosed Cylinder-Flare Bodies," LMSC 667991, Dec. 1958.

[19] Reding, J. P. and Ericsson, L. E., "Static Loads on the Saturn I-Apollo Launch Vehicle," LMSC-803185, Aug. 1963.

[20] Coe, C. F. and Nute, J. B., "Steady and Fluctuating Pressures at Transonic Speeds on Hammerhead Launch Vehicles," NASA TM X-778, Dec. 1962.

[21] Robertson, J. E. and Chevalier, H. L., "Characteristics of Steady-State Pressures on the Cylindrical Portion of Cone-Cylinder Bodies at Transonic Speeds," AEDC TDR 63-104, Aug. 1963.

[22] Chevalier, J. E. and Robertson, J. E., "Pressure Fluctuations Resulting from Alternating Flow Separation and Attachment at Transonic Speeds," AEDC TDR 63-204, Nov. 1963.

[23] Ericsson, L. E., "Aeroelastic Instability Caused by Slender Payloads," *Journal of Spacecraft and Rockets,* Vol. 4, Jan. 1967, pp. 65-73.

[24] Bisplinghoff, R. L., Ashley, W., and Halfman, R. L., *Aeroelasticity,* Addison Wesley, Cambridge, Mass., 1955, pp. 418-419.

[25] Flynn, J., private communication of Seasat-A maximum α history including winds, Lockheed Missiles & Space Co., Inc., Nov. 1976.